

Contents list available at CBIORE journal website

F RE International Journal of Renewable Energy Development

Journal homepage: https://ijred.cbiore.id



Research Article

Boosting thermal regulation of phase change materials in photovoltaicthermal systems through solid and porous fins

Sura A. Namuq[®] and Jasim M. Mahdi[®]

Department of Energy Engineering, University of Baghdad, Baghdad, Iraq

Abstract. This study explores the integration of porous fins with phase-change materials (PCM) to enhance the thermal regulation of photovoltaic-thermal (PVT) systems. Computational simulations are conducted to evaluate the impacts of different porous fin configurations on PCM melting dynamics, PV cell temperatures, and overall PVT system effectiveness. The results demonstrate that incorporating optimized porous fin arrays into the PCM region can significantly improve heat dissipation away from the PV cells, enabling more effective thermal control. Specifically, the optimized staggered porous fin design reduces the total PCM melting time and decreases peak cell temperatures by about 5°C. This is achieved by creating efficient heat transfer pathways that accelerate the onset of natural convection during the PCM melting process. Further comparisons with traditional solid metallic fins indicate that while solid fins enable 12.2% faster initial melting, they provide inferior long-term temperature regulation capabilities compared to the optimized porous fins. Additionally, inclining the PV module from 0° to 90° orientation can further decrease the total PCM melting time by 13 minutes by harnessing buoyancy-driven convection. Overall, the lightweight porous fin structures create highly efficient heat transfer pathways to passively regulate temperatures in PVT systems, leading to quantifiable improvements in thermal efficiency of 16% and electricity output of 2.9% over PVT systems without fins.

Keywords: PVT system; PCM, Thermal control; Porous fins; Solid fins; Melting



@ The author(s). Published by CBIORE. This is an open access article under the CC BY-SA license (http://creativecommons.org/licenses/by-sa/4.0/). Received: 29th Oct 2023; Revised: 28th Dec 2023; Accepted: 2nd Jan 2024; Available online: 5th Jan 2024

1. Introduction

Photovoltaic-thermal (PVT) systems have garnered substantial research efforts in the last few years owing to their capacity to concurrently harvest electrical and thermal energy from incident solar irradiation (Al-Aasama et al., 2023). However, excessive heating within Photovoltaic (PV) cells during peak operational hours remains a critical impediment challenging widespread PVT implementation. PV cells generally have a limited conversion efficiency of sunlight to electrical power of up to 20%, and the rest is transformed into wasted heat. This residual heat build-up can cause module temperatures to exceed 80°C or 100°C in warmer areas (Ma, Yang, Zhang, Lu, & Wang, 2015). This declines the electrical efficiency by 0.5% for each 1°C above the recommended operating temperature of 25°C and accelerates cell deterioration (Kant, Shukla, Sharma, & Biwole, 2016; Sharma et al., 2017). One approach to addressing this challenge is to use phase-change materials (PCMs) for thermal control. PCMs can absorb and release large amounts of heat during their phase transition, making them an attractive option for regulating the temperature of PV and PVT systems. (Wagas & Ji, 2017) investigated the influence of PCMs on PV performance throughout seasons. Their findings revealed that the temperature of the PV cells dropped by 21.2 °C in June, while the efficiency climbed by 9%. (Thaib, Rizal, Mahlia, & Pambudi, 2018) showed that using a PCM boosted the photoelectric production rates of PV module from 6.1-6.5% to 7.0-7.8%. They

also discovered that using PCM not only reduced the temperature of PV cells yet additionally reduced variations in temperature, enhancing the consistency of the generated electricity and the longevity of cells.

Despite beneficial thermal regulation capabilities, PCMs' poor conductivity causes substantial temperature gradients, hindering effectiveness. Proposed solutions involve bundling PCM-filled tubes on module rear sides (Indartono, Prakoso, Suwono, Zaini, & Fernaldi, 2015; Kılkış, 2020; Li et al., 2022; Maatallah, Zachariah, & Al-Amri, 2019; Wagas, Jie, & Xu, 2017), reducing cell temperatures and increasing PV efficiency. Alternatively, nanoparticles can enhance PCM-based thermal control. Studies found nanoparticles enabled efficient regulation, performance, improved higher electrical/thermal efficiency (Al-Waeli et al., 2018; Al-Waeli et al., 2017; Jamil et al., 2021; Ma, Lin, & Sohel, 2016; Nada, El-Nagar, & Hussein, 2018; Nižetić, Jurčević, Arıcı, Arasu, & Xie, 2020). Another simpler, feasible approach is integrating metallic fins into PCMs. Investigations revealed PV/PCM systems with metal fins cut peak cell temperatures by up to 15°C and elevated output by about 5.39% versus air-cooled PVs (Tan, Date, Fernandes, Singh, & Ganguly, 2017). (Khanna, Reddy, & Mallick, 2018a) revealed that installing metallic fins in a PV-PCM system boosted power generation in both warm and cold conditions by about 1% and 6.7%, respectively. (Ren, Xu, & Luo, 2019) demonstrated that metallic fins have better potential to accelerate the PCM melting over nanoparticles. Among past enhancement techniques, porous foams

^{*} Corresponding author Email: jasim@siu.edu (Jasim M. Mahdi)

exceptional thermal efficiency owing to high surface-area-tovolume ratios, negligible weight, and permeability/stability. Numerous studies confirm their efficacy. (Cheong Tan et al., 2019) investigated the use of porous aluminium as a heat sink in concentrated photovoltaic (CPV) modules to improve heat dissipation. Their results showed that the porous aluminium significantly improved the heat dissipation and temperature of the CPV module. (Duan, 2021) examined the efficacy of PCM included with a porous metallic structure for passive PV cooling at 20 °C. When a porous PCM system is used as a heat sink, the results confirmed that the cooling potential is greatly increased over natural PCM. (Sharaf, Huzayyin, & Yousef, 2022) showed that applying aluminium foams to PV-PCM systems resulted in 4% lower temperatures and 1.85% higher energy yield over conventional PV systems. (Shakibi, Afzal, Shokri, & Sobhani, 2022) found that the integration of aluminium foams into PVT-PCM systems enhanced heat dispersion, cutting temperatures by up to 7°C while elevating electrical performance by about 13.8% at the porosity level of 0.80.

Despite extensive research efforts on porous foams and solid fins, a gap persists regarding the use of porous fins within PCM components for thermal regulation of PVT systems. This study investigates integrating porous fins in PCM to optimize the potential of PVT system for thermal regulation. Localized porous fins provide higher surface area versus solid fins while preventing high flow impedance of fully porous foams. During melting, the reduced flow impedance promotes natural convection. Additionally, utilizing localized porous fins minimizes costs by necessitating less porous material weight. This curtails the reduction in usable PCM volume accessible to thermal storage, enabling more effective leveraging of heat dissipation capabilities in the PVT system. Herein, computational fluid-dynamic simulations conveyed to advance PVT thermal performance through porous fin distribution, tilt angle optimization, and benchmarking against solid fins. The outcomes would establish design guidelines to leverage porous fins in PCM encapsulations for enhancing real-world PVT effectiveness and scalability, expediting widespread implementation.

2. Methodology and simulation

2.1 Geometry and Problem Details

The system in charge consists of a PVT collector enclosed in an aluminium container filled with a PCM and an embedded porous fin assembly for thermal enhancement (Figure 1). Aluminium was selected for its high degree of thermal

conductivity, which allows for efficient conductive heat transmission from the PV panel to the PCM layer. However, the poor thermal conductivity and sluggish thermal response of PCM restrict heat transfer effectiveness. To solve this issue, porous or solid fins are integrated into the PCM region to boost heat transfer rates and thermal dissipation capabilities. The localized porous fins provide higher surface area compared to solid fins while preventing the high flow impedance of fully porous foams. During melting, the reduced flow impedance promotes natural convection heat transfer within the liquid PCM. Additionally, using localized porous fins minimizes required porous material weight, reducing manufactured costs. This enables more effective leveraging of heat dissipation potential within the PVT system.

RT35 was chosen as the PCM for this research due to its melting point of 308 K (35°C), which makes it well-suited for regulating the PV cell temperatures during typical operating conditions. Additionally, RT35 has a suitable phase transition enthalpy of 148 kJ/kg that enables substantial absorption of heat from the PV cells as it undergoes melting. These favourable thermophysical characteristics would enable RT35 to serve as an effective PCM for PV thermal regulation (Table 1).

The porous fins comprised aluminium foam structures with an overall fin surface area of approximately 150 cm². Porosity is described as the amount of pore space to the total space in the porous fins. The analysis focused on optimizing the photovoltaic cell design by examining the effects of porosity levels in the porous fins to balance heat transfer and PCM volume for thermal management. Table 2 lists the nominal thermophysical characteristics of PV cells employed in the suggested PVT system. The tilt angles analysed for the system were 0°, 30°, and 90° to explore angle sensitivity.

2.2 Mathematical description

This section concerns the development of the mathematical model for analyzing the thermal performance of PVT system with porous fins and PCM using the enthalpy-porosity approach. This method includes Darcy's law to allow flow across porous medium with the Kozeny-Carman equation for simulating the fluid dynamics in melting PCM. It simplifies the energy equations during both PCM solid and liquid phases, eliminating the need to track liquid-solid interface evolution. The phase change boundary is determined via the liquid fraction computed in grid cells, denoting the cell volume fraction occupied by liquid versus the entire cell area. Additionally, the mushy zone with liquid fractions between 0-1 is modeled as a porous medium with evolving porosity during melting. Heat transfer initially

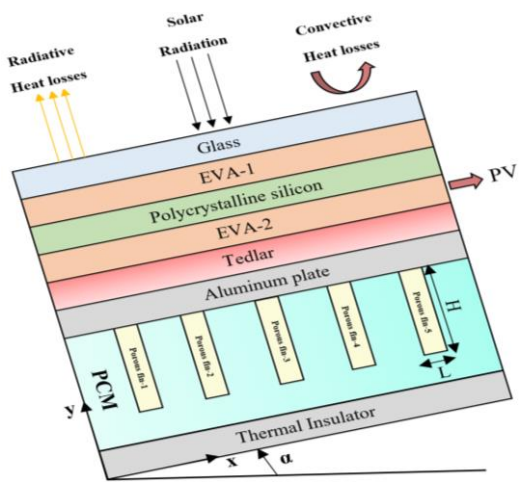


Fig 1. PVT design using PCM and porous fins.

Table 1Thermophysical features of PCM, porous fins employed and Aluminium plates in the suggested PVT system

Property	PCM	Porous fins (Al6061)	Aluminium plates	
	(RT-35)(GmbH.)			
$\rho_{\rm m}[{ m kg/m^3}]$	770	160	2700	
C _P [J/kg. K]	2000	896	870	
K[W/m.K]	0.2	167	202	
Thickness[mm]	-	-	2	
L[kJ/kg]	148	-	-	
$T_s[K]$	302	-	-	
$T_{l}[K]$	308	-	-	
β[1/K]	0.0006	-	-	

Table 2

Thermophysical features of PV cell employed in the suggested PVT system

Property	PV cell(Waqas, Ji, Xu, Ali, & Alvi, 2018)	EVA(Waqas et al., 2018)	Tedlar (Waqas et al., 2018)	Glass(Waqas et al., 2018)
$\rho_{\rm m}[{\rm kg/m^3}]$	2330	960	1200	3000
$C_{P}[J/kg. K]$	677	2070	1250	500
K[W/m.K]	148	0.3	0.2	2
Thickness[mm]	0.2	0.5	0.3	3

occurs by conduction. However, upon melting commencement, density-driven natural convection becomes significant. The porous fins assist melting initiation, while convection supplements conduction, accelerating the melting rate. To ensure computational tractability, several simplifying assumptions are employed:

- 2D heat transfer at the x-y coordinates
- Laminar, incompressible, Newtonian flow of liquid PCM
- Isotropic and homogeneous porous fins with open cells
- PCM and porous fins are in local thermal equilibrium
- Boussinesq approximation is valid for density estimation
- Solar irradiation is uniform at the PV upper surface

With these assumptions, the model can be solved iteratively to elucidate the thermofluidic behaviour within the finned PVT system, enabling investigation of the parameters influencing effectiveness.

2.2.1 Governing equations

Continuity equation:

The continuity equation, expressed as Eq. (1), is formulated using the above assumptions as (Mahdi, Lohrasbi, Ganji, & Nsofor, 2018).

$$\frac{\partial \rho_f}{\partial t} + \nabla \cdot \rho_f V = 0 \tag{1}$$

Momentum equation:

Eqs (2-3) provide the momentum equations for the x and y-plane (Mahdi et al., 2018).

$$\frac{\rho_f}{\varepsilon} \frac{\partial u}{\partial t} + \frac{\rho_f}{\varepsilon^2} (V \cdot \nabla u) = -\frac{\partial P}{\partial x} + \frac{\mu_f}{\varepsilon} (\nabla^2 u) - A_m \frac{(1-\lambda)^2}{\lambda^3 + \delta} u - \left(\frac{\mu_f}{\kappa} + \frac{\rho_f C_f |u|}{\sqrt{\kappa}}\right) u \tag{2}$$

$$\frac{\rho_f}{\varepsilon} \frac{\partial v}{\partial t} + \frac{\rho_f}{\varepsilon^2} (V \cdot \nabla v) = -\frac{\partial P}{\partial y} + \frac{\mu_f}{\varepsilon} (\nabla^2 u) - A_m \frac{(1-\lambda)^2}{\lambda^3 + \delta} v - \left(\frac{\mu_f}{K} + \frac{\rho_f C_f |v|}{\sqrt{K}}\right) v - \rho_f g \beta \varepsilon (T - T_{ref})$$
(3)

The second and third components on the right part of the momentum equations include viscous resistance and the Kozeny-Carman coefficient, accordingly. The fourth and fifth parameters represent the extension of Darcy's law to include non-Darcy phenomena. The sixth term represents the Boussinesq estimate, which takes into account an opposing direction of acceleration caused by gravity in the y- plane. This element is represented as $\rho_f g \beta \epsilon$ (T-Tref), where ρ_f denotes density, g is gravity's accelerating, β is the thermal expansion coefficient, and T_{ref} is a reference temperature.

Energy equation

The energy balance formula dependent on the thermal equilibrium between the PCM and porous fins is shown in Eq. (4) as (Mahdi & Nsofor, 2018):

$$\begin{split} \left[\varepsilon \left(\rho C_{p}\right)_{f} + (1-\varepsilon) \left(\rho C_{p}\right)_{s}\right] \frac{\partial T}{\partial t} + \left(\rho C_{p}\right)_{s} (V.\nabla T) &= K_{e} \nabla^{2} T - \varepsilon (\rho L)_{f} \frac{\partial \lambda}{\partial t} \end{split} \tag{4}$$

Here, ϵ represents porosity, and $(\rho C_p)_f$ and $(\rho C_p)_s$ represent the fluid and solid phase specific heats, accordingly. T is the temperature, V is the speed vector, $\partial \lambda/\partial t$ is the liquid fraction time derivative Ke is the effective thermal conductivity. The subscript "s" represents the porous fin, while the subscript "f" represents the PCM in both liquid and solid forms. Other parameters used in the equations involve u for the x-axis velocity component, v for the axis velocity component, P for pressure, μ_f for dynamic viscosity, A_m as a mushy zone fixed, and C_f for the Kozeny-Carman coefficient. Furthermore, the variables δ,λ,K , are described as follows:

δ : A small coefficient with a value of 0.001.

 λ : The liquid fraction, determined by equation (5):

$$\lambda = \begin{cases} 0 & T \leq T_{solid} \\ T - T_{solid} / T_{liquid} - T_{solid} & T_{solid} < T < T_{liquid} \\ 1 & T \geq T_{liquid} \end{cases}$$
 (5)

K: Permeability of the porous fins, calculated using equation (6) (Calmidi & Mahajan, 2000):

$$\frac{\kappa}{d_p^2} = 0.00073(1 - \varepsilon)^{-0.224} \left(\frac{d_l}{d_p}\right)^{-1.11} \tag{6}$$

$$C_f = 0.00212(1 - \varepsilon)^{-0.132} \left(\frac{d_l}{d_p}\right)^{-1.63}$$
 (7)

The porosity ε , ligament diameter d_l and pore density ω are the essential factors that comprise the structural characteristics of porous fins (Calmidi & Mahajan, 2000). d_l/d_p is the ratio of ligament diameter (d_l) to pore size (d_p), computed as follows equation (8):

The porosity ε , pore density ω and ligament diameter d_l the ligament diameter are the fundamental parameters that

$$\frac{d_l}{d_p} = .18 \sqrt{\frac{1-\varepsilon}{3\pi}} \left(\frac{1}{1-e^{-(1-\varepsilon)/0.04}} \right) \tag{8}$$

Where $d_p = 0.0254(m)/\omega(PPI)$

 K_{ν} : The effective thermal conductivity for the PCM-porous fin combination was obtained utilizing equation (9) (Tian & Zhao, 2011)

$$K_{v} = \frac{\sqrt{2}}{2(M_{A} + M_{B} + M_{C} + M_{D})} \mid k_{s=0}$$
 (9)

Where: M_A , M_B , M_C , M_D are factors, which were used to shorten these formulations. The values of these variables are calculated from the equations (10)-(13), which are as follows:

$$M_A = \frac{4\sigma}{(2e^2 + \pi\sigma(1-e))k_s + (4-2e^2 - \pi\sigma(1-e))k_f}$$
(10)

$$M_B = \frac{(e-2\sigma)^2}{(e-2\sigma)e^2k_s + (2e-4\sigma - (e-2\sigma)e^2)k_f}$$
(11)

$$M_C = \frac{(\sqrt{2} - 2e)^2}{2\pi\sigma^2(1 - 2e\sqrt{2})k_s + 2(\sqrt{2} - 2e - \pi\sigma^2(1 - 2e\sqrt{2}))k_f}$$
(12)

$$M_D = \frac{2e}{e^2 k_s + (4 - e^2) k_f} \tag{13}$$

Where e = 0.339 and σ is the parameter of porous fins that can be estimated by equation (14):

$$\sigma = \sqrt{\frac{\sqrt{2}(2-5/e^3\sqrt{2}-2\varepsilon)}{\pi(3-4e\sqrt{2}-e)}}$$
 (14)

2.2.2 PVT structure

A large amount of incident solar radiation is transformed to inefficient heat during the PV operation. This heat is lost to the surroundings through radiation and convection by the upper glass covering. The amount of heat loss is determined by a number of elements, including the emissivity and absorption of the PV layer substances, the convection rate of heat transfer coefficient, and the temperature of the ambient air. The thermal energy balance on the PV's top layer is given as (Mahdi, Singh, Al-Najjar, Singh, & Nsofor, 2021):

$$-k_{glass} \frac{\partial T}{\partial y} = (h_{forced} + h_{natural})(T_{amb} - T_{glass}) + \epsilon_{glass} \sigma (T^4_{sky} - T^4_{glass})F + \alpha_{pv}I_{pv}(1 - \eta_{pv})$$
(15)

Here, $\partial T/\partial y$ represents the temperature range , k_{glass} is the thermal conductivity of the glass, , $h_{natural}$ and h_{forced} are the natural and forced convection heat transfer coefficients. σ is

the Stefan-Boltzmann constant (5.6697 \times $10^{\text{-8}}$ W/m².K⁴), ε_{glass} is the emissivity of the glass cover, α_{pv} represents the transmissivity of the solar , F is the radiation shape factor. cell: EVA layers and glass multiplying with the silicon absorptivity. In this study, it is estimated as (0.9). I_{pv} is the solar radiation intensity, and η_{pv} is the efficiency of the PV cell that determined by equation (16) (Kaplani & Kaplanis, 2014; Mahdi, Mohammed, & Talebizadehsardari, 2021)

$$\eta_{pv} = \eta_{st} \left(1 - \beta_{st} (T_{glass} - T_{st}) \right) \tag{16}$$

Where η_{st} is the standard efficiency of cells ($\eta_{st}=0.171$) as given by manufacturer; β_{st} is the standard coefficient of temperature for the PV panel ($\beta_{st}=0.45\times 10^{-2}$) and T_{st} is the normal temperature for operation of PV cells ($T_{st}=25^{\circ}$ C). The energy charge rate is calculated, which reflects the capability of thermal energy control per unit of melting time. (Xu, Ren, Zheng, & He, 2017)

$$\dot{Q_m} = \frac{(m_{pcm}) \left((c_{P,s})_{pcm} (T_l - T_{int}) + L + (c_{P,l})_{pcm} (T_{end} - T_l) \right)}{t_m}$$
(17)

Here, Q_m is the PCM system's energy charging capacity, which consists of the sensible heat for solid PCM, latent heat of melting, and sensible heat for liquid PCM; T_{ini} and T_{end} are the average temperatures of the PCM at the start and ending of the thermal management process, respectively. m is the PCM's mass. Take note that the initial temperature is 293 K. Another essential statistic for the thermal effectiveness of the PVT system is its thermal performance.

$$\eta_{TH} = \frac{\dot{Q}_m}{IA_{pv}} \tag{18}$$

Here, A_{pv} is the surface area of the PV module.

2.2.2.1 Radiative heat losses

The radiation heat loss caused by the PV top surface is dictated by the (T_{sky}) , (T_{amb}) , (ϵ_{glass}) emissivity of the surface (glass), F radiation shape parameter panel angle of tilt(α). The entire quantity of radiation heat transfer may be computed as follows (Bergman, Bergman, Incropera, Dewitt, & Lavine, 2011):

$$q_{sky} = \epsilon_{glass} F \sigma A (T_{glass}^{4} - T_{sky}^{4})$$
(19)

$$T_{sky} = (0.037336T_{amb}) + (0.32T_{amb}) \tag{20}$$

$$F_{sky,front} = \frac{1 + \cos \alpha}{2} \tag{21}$$

$$F_{base,front} = \frac{1 - \cos \alpha}{2} \tag{22}$$

2.2.2.2 Convective heat losses

The PVT system dissipates heat at the upper surfaces of the photovoltaic panels by forced and free convection. The entire quantity of heat losses may be calculated using Newton's cooling equation (Al-Waeli, Kazem, Chaichan, & Sopian, 2019).

$$q_{conv} = (h_{free} + h_{forced})A(T_p - T_{amb})$$
(23)

where $T_p = T_{glass}$ to heat loss from the PV upper side.

The measure of the coefficient of free convection heat transfer between either side of the panel is determined as follows by (Skoplaki & Palyvos, 2009).

$$h_{free} = \left(\frac{\frac{0.67(\cos\alpha)Ra^{0.25}}{\left(\left(\frac{0.492k}{\mu c_p}\right)^{\frac{9}{16}}+1\right)^{0.44}} + 0.68}{\left(\left(\frac{0.492k}{\mu c_p}\right)^{\frac{9}{16}}+1\right)^{0.44}} + 0.825\right) \frac{k}{\ell} \text{ For Ra} \le 10^9$$

$$h_{free} = \left(\frac{\frac{0.387Ra^{0.167}}{\left(\left(\frac{0.492k}{\mu c_p}\right)^{\frac{9}{16}}+1\right)^{0.44}} + 0.825}{\left(\left(\frac{0.492k}{\mu c_p}\right)^{\frac{9}{16}}+1\right)^{0.44}} + 0.825\right) \frac{k}{\ell} \text{ For Ra} > 10^9$$
(25)

$$h_{free} = \left(\frac{\frac{0.387Ra^{0.167}}{\left(\left(\frac{0.492k}{\mu cp}\right)^{\frac{9}{16}} + 1\right)^{0.44}} + 0.825\right) \frac{k}{\ell} \text{ For Ra} > 10^9$$
 (25)

$$Ra = \frac{g\beta_{air}\ell^3\rho^2c_p}{k\mu}(T_{panel} - T_{amb})$$
 (26)

$$\beta_{air} = \left(\frac{\partial \rho}{\partial T_{nanel}}\right) \frac{1}{\rho} \tag{27}$$

Ra is the Rayleigh number, and ℓ is the characteristic length of the PV module β_{air} is the thermal expansion coefficient of air, T_{amb} and T_{panel} are the temperature of the PV module and temperatures of the panel surface, respectively.

The experimental relationships for the coefficient of forced convective heat transfer (h_{forced}) and according to $Re = \frac{\rho v \ell}{u}$ are supplied by (Skoplaki & Palyvos, 2009).

$$h_{forced} = \frac{k}{\ell} \frac{0.3387 p r^{\frac{1}{3}} (Re)^{\frac{1}{2}}}{\left(1 + \left(\frac{0.0468}{pr} (Re)^{\frac{2}{3}}\right)^{\frac{1}{4}}}\right)} \text{ For } Re \le 10^5$$
 (28)

$$h_{forced} = 2\frac{k}{L}Pr^{\frac{1}{3}}(0.037Re^{\frac{4}{5}} - 871)$$
 For $Re > 5 \times 10^5$ (29)

$$\left(P_r = \frac{c_p \mu}{K}\right) \tag{30}$$

2.3 Initial and boundary condtions

- The solar irradiance intensity is Isolar = 1000 W/m² at the PV front side.
- At t=0, the PCM part has a standard temperature $(T_{int} = 293 \text{ K}).$
- The PCM areas' borders are regarded as thermally insulated.
- Aluminum foam fins with a porosity value of ($\varepsilon = 0.85$) are evaluated.

Numerical approach and validation 3.

To examine the thermal regulation potential of PCM combined with porous fins in the proposed PVT system, numerical simulations were performed using Ansys Fluent 21.1. The study investigated the phase change behavior of PCM within aluminum porous fins. The thermal equilibrium porous media approach was used for the solidification/melting formulation, based on an enthalpy-porosity equation. Additionally, the mushy zone, containing alternating PCM liquid and solid phases, was modeled as a porous medium with evolving porosity during melting. Solar irradiation was applied and convection/radiation losses were accounted for on the upper PV surface. Furthermore, the governing equations were implemented using the FLUENT solver's C++ user-defined function (UDF).

The SIMPLE scheme computed for the combined velocity and pressure, while the Green-Gauss node-based method computed for gradients. The PRESTO and QUICK schemes

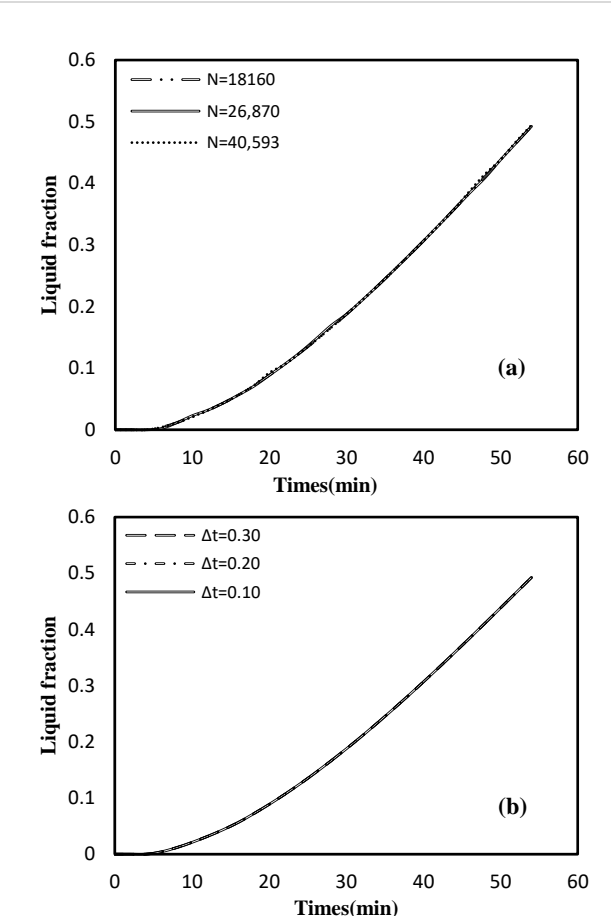


Fig 2. Solution independence test for (a) the grid size and (b) the time step on the progress of PCM melting.

calculated pressure and momentum/energy, respectively. Under-relaxation factors for pressure, momentum, liquid fraction, and energy were 0.3, 0.5, 0.7, and 1. To ensure solution autonomy, time step size and mesh density were investigated. Three mesh sizes (18157; 26870; 40593) were tested, with 18160 elements selected for saving simulation time while maintaining consistent liquid fraction characteristics. Additionally, various time steps (0.10 s, 0.20 s, 0.30 s) were evaluated to determine the best value (Figure 2), which was 0.30 s for preserving solution independence and consistency during melting. For the convergence criterion, residuals for the continuity, momentum, and energy equations were set to 10⁻⁶, 10⁻⁴, and 10⁻⁴.

3.1 Validation

The aim of this section is to verify the simulation correctness and dependability in use by comparing the results to experimental findings from (Biwole, Eclache, & Kuznik, 2013). The research employed boundary conditions and thermophysical properties for the PCM system identical to the original study. Figure 3 illustrates a comparison between the predicted temperature profiles of the PV cells over time and the corresponding experimental results. The consistency between the projected values and experimental data validates the dependability and correctness of the simulation model. The simulation conducted for the container with PCM being heated by solar radiation penetrating via the top of the PV module and cooled by heat transport to the surroundings. Based on the validated model, the numerical results, including time evolution of temperature distribution, PV cell temperature, thermal regulation period, and electrical power efficiency of the PV module, were provided and analysed in detail.

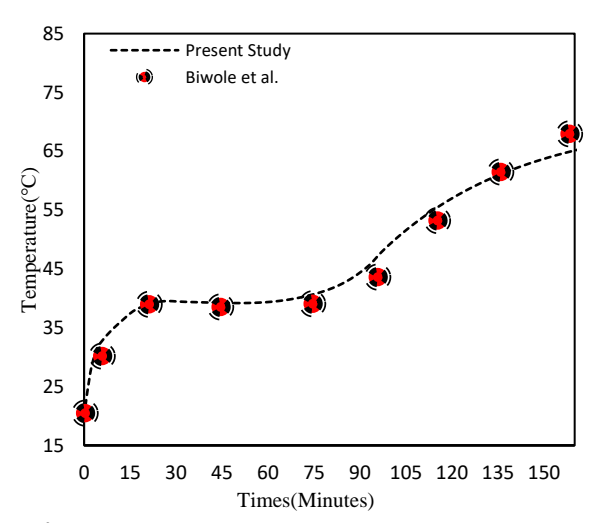


Fig 3. Validation of simulation-based PV temperature distributions versus experimental findings from (Biwole *et al.*, 2013)

4. Results and Discussion

The numerical model developed in the previous section was employed to conduct the required series of numerical simulations. These simulations provided important insights into using porous fins with PCMs to improve the thermal regulation potential of the PVT system. The study systematically explored three main factors, which are: porous fin arrangement, tilt angle, and comparison to solid fins to understand how they impact heat transfer and PCM melting in the PVT system.

The PV thermal regulation scenario starts when the PCM is in a solid phase at a temperature of 20°C (293K) and a solar radiation constant equal to 1000 w/m². The radiation that enters encourages the melting of the PCM located beneath the PV module, as presented in Figure 1. As time passes, the existence of porous fins rises heat transfer through the PV side to the PCM aspect, increasing the change in phase of the PCM and permitting it to utilize more heat produced in the PV panels, leading to enhanced operation.

4.1 Influence of the porous fins distribution on the PVT-PCM system

This section involves the influence of porous fins distribution on the thermal performance of PCM in the proposed PVT system. Five cases were examined including the original (Case A) that features no porous fins to serve as a baseline for comparison against other Cases B-C-D-E, which had irregular fin spacing, as seen in Figure 4. The fin size in these cases was kept constant for meaningful comparisons, with a porosity of ϵ = 0.85 and a pore density of 10 PPI. The fin spacing's in these cases are summarized in Table 3.

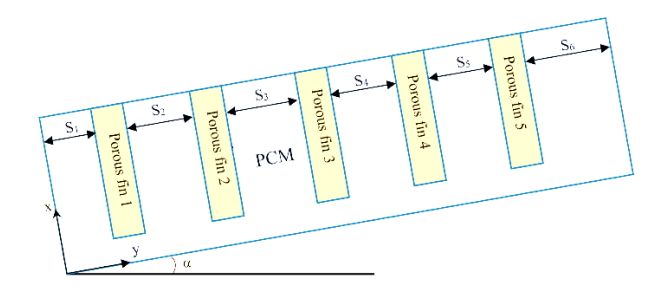


Fig 4. Schematic of the geometric distribution of the proposed porous fin arrays

Table 3Values of fin spacing in the studied fin arrays

	S1	S2	S3	S4	S5	S6
	(mm)	(mm)	(mm)	(mm)	(mm)	(mm)
Case B	16	10	36	20	10	8
Case C	5	5	75	5	5	5
Case D	6	5	12	27	20	30
Case E	5	13	50	24	5	3

An in-depth analysis of Figure 5 indicates distinct trends in the progression of PCM melting dynamics stemming from adjustments in porous fin distribution within the PVT system. Incorporating fins visibly accelerates early-stage heat absorption from the PV cell relative to the baseline scenario devoid of regular fin distribution, as evidenced by the broader expansion of melted PCM zones (red) surrounding the fins at the 30-minute mark across Cases B through E. However, more differences become increasingly apparent between the various fin arrangements over more prolonged heating periods. Specifically, the irregular distribution of fins in Cases B-E drives more nonuniform melt patterns, with sizable PCM volumes persisting largely in the solid phase within the mid and lower portions of the domain after 90 minutes of sustained solar irradiation at the upper PV surface. Notably, Case D exhibits appreciably faster and more homogeneous melting behaviour attributed to its optimized inter-fin spacing, which effectively bolsters natural convective currents within the liquefied PCM domain. In contrast, the irregular but suboptimal fin spacing in Cases B, C, and E seems to impede heat transfer contributable to convection, hampering the bulk melting rates, and diminishing the overall thermal regulation capacity. Meanwhile, the scenario of using pure PCM alone (Case A)(Biwole et al., 2013) provides relatively poorer thermal control regulation capabilities because the absence of porous fins. Overall, the quantifiable metrics reveal Case D reduces the total duration for complete PCM melting by 50 minutes, or 45%, compared to the non-finned scenario. This substantiates the positive influence of strategic fin integration on accelerating phase change processes.

Complementary temperature contour profiling in Figure 6 provides more critical insights into the impacts of inter-fin spacing on heat diffusion traits over time. Initially, the high heat flux output from the PV cell is conducted into the PCM region through the fins across all spacing variants, fostering the establishment of sizable temperature gradients near the panel and fins as conveyed visually via the color spectrum spanning yellow to red hues. The magnitude of these gradients progressively rises with heating time, especially upon descending below vertical tilt angles of 90°. However, a pivotal observation is the superior temperature uniformity sustained within the red layer for the 90° inclination angle in Case D after 60 minutes. After 90 minutes, pronounced thermal variations become clearly evident under non-optimized fin spacing arrangements in Cases B and C over extended melting durations. Quantitatively, this no uniformity culminates in localized temperature elevations approaching 38°C on the PV panel, whereas Case D restricts peak readings to nearly 36°C. Thus, good fin distribution gives rise to appreciable cell temperature reductions relative to the pure PCM scenario, conferring dual advantages of enhanced electrical efficiency and lifespan prolongation.

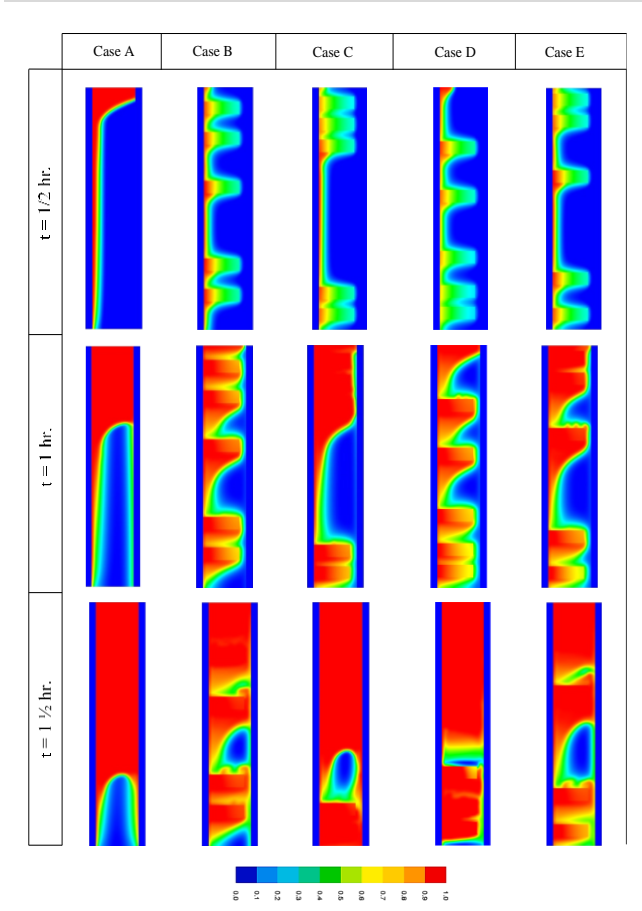


Figure 5: Contours for the liquid fraction over different time periods through PCM melting with varying distributions of porous fins

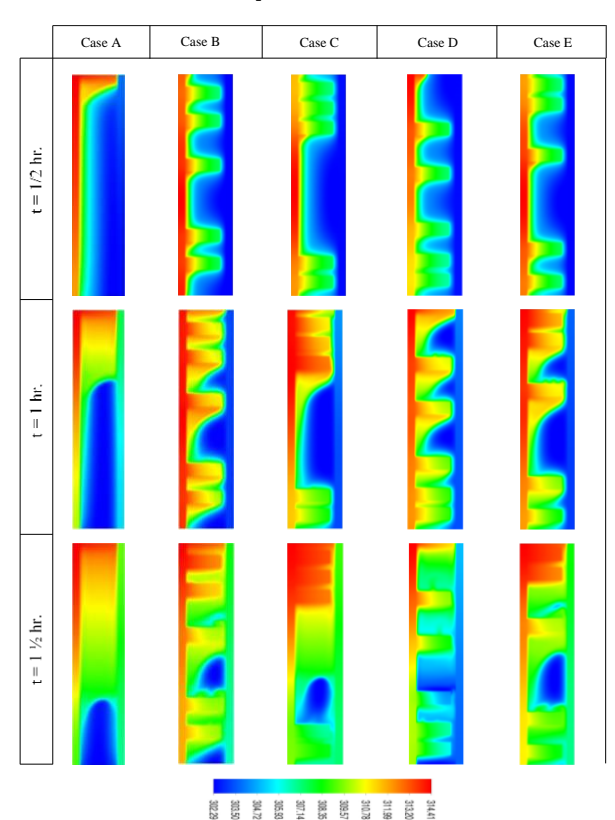
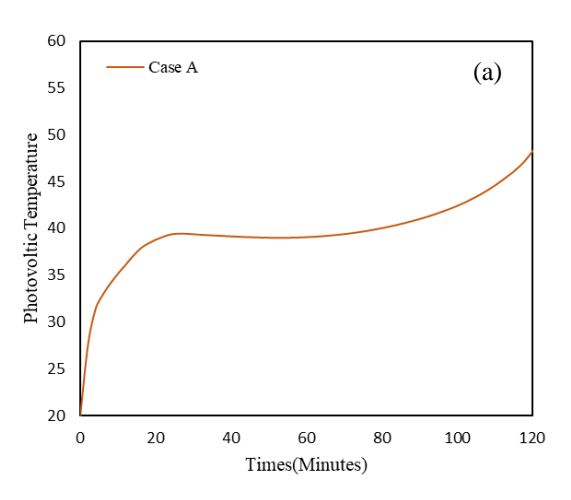


Fig 6 Contours for the temperature distribution over different time periods of PCM melting with varying distributions of porous fins

Figure 7 depicts the average temperature profiles of the PV cells while under thermal control of the porous fins included in

the PVT system. This is contrasted to the temperature distribution for a PVT system with no porous fins. Figure 7(a) illustrates the temperature curve of a PV cell cooled solely with PCM, excluding the use of porous fins. The temperature of the PV cell rises from 293 K (20 °C) to attain a temperature equilibrium around 313 K (40 °C). In contrast In Figure 7 (B), the temperature profile for Case D with optimized irregular fin spacing remains highly stable over time, maintaining a temperature around 309K (36°C). This indicates excellent thermal regulation of the PV panel. In contrast, Cases B, C, and E with irregular fin spacing show sustained PV temperature increases beyond 1 hr, suggesting deficient heat dissipation from the PV cell. Case D's optimized fin spacing enhances conductive heat transfer into the PCM, enabling superior thermal regulation. It would be worth mentioning that the periods where the temperature curves plateau in Figure 7 because the system reaches thermal equilibrium temporarily during the phase change process before temperature continues rising. Specifically, when the PCM starts melting, the temperatures increase initially and then stabilize as the PCM absorbs heat. Once the PCM is fully melted, temperatures climb again until reaching the next equilibrium stage. Overall, the analysis of temperature data in Figure 7 clearly demonstrates that Case D's fin distribution enables the best thermal performance, maintaining a stable PV temperature over a longer period of time for the PV thermal regulation.



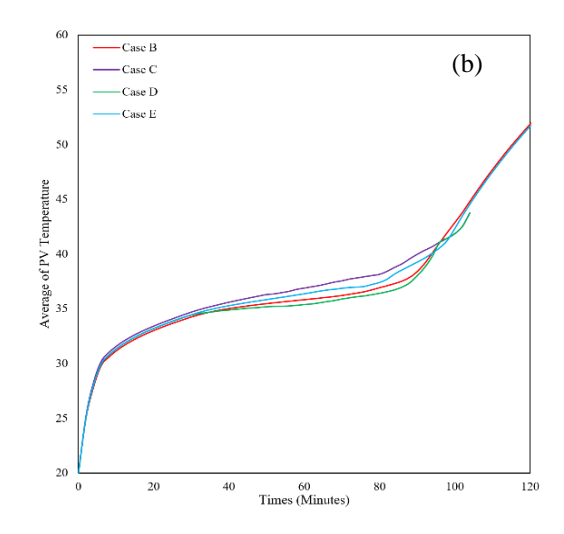


Fig 7. Temperature charts of PV cells for (a) only PCM component (b) different distribution of porous fins in PCM.

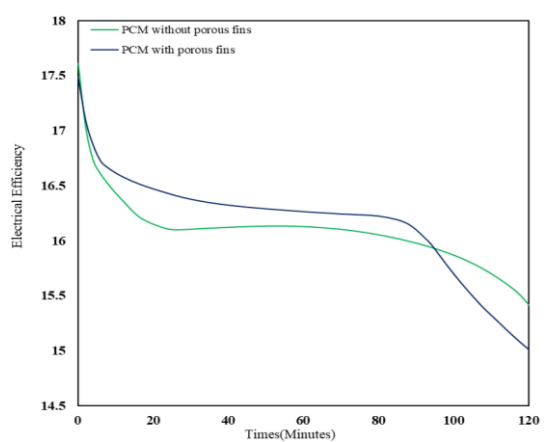


Fig 8. The effect of porous fins on the electrical performance of a PVT system

The electrical efficiency profiles in Figure 8 display pivotal electrical performance divides stemming from the integration of porous fins within the PCM domain of the PVT system. Initially, both configured PVT variants exhibit rising electrical efficiency profiles as a fraction of absorbed irradiation gets converted into useful electric output while the remainder manifests as waste heat. However, their developmental trajectories soon diverge as the impact of overheating builds within the PV cell in the absence of adequate heat dissipation pathways. Meanwhile, employing porous fins with an ideal fin arrangement (Case D), the performance maintains higher trends while the PCM takes heat from the PV cell through porous fins, thus maintaining the optimal PV temperature. This suggests that the porous fins provide good temperature regulation. However, without fins, efficiency gradually declines as heat accumulates in the panel, lowering efficiency. More importantly, if the PCM completely melts after about 1.5 hours, the performance of the system without fins will decrease significantly as the temperature on the solar panel rises rapidly. However, with the fins, the performance remains stable according to the improved heat transfer through the fins to the PCM; this enables greater heat control after full melting. The average electrical efficiency gain of the PVT with porous fins is 2.98% compared to the case with no porous fins. This means the porous fins provide greater electrical efficiency by removing heat inside the PV module and reducing temperature.

Figure 9 represents the thermal efficiency of a porous fin PVT system through time. Porous fins with PCM have a substantial impact on thermal efficiency, and preliminary findings propose the greatest possible efficiency owing to a rise

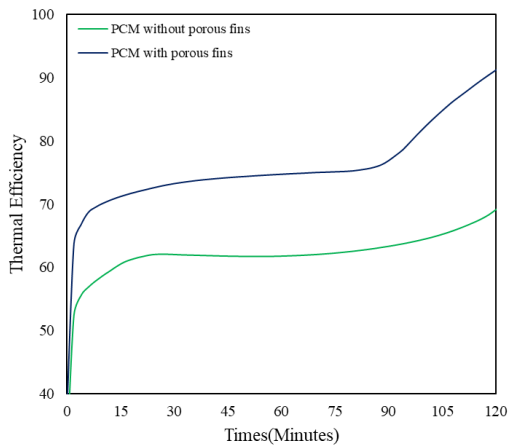


Fig 9. The effect of porous fins on the thermal performance of a PVT system

in the latent heat for melting. The porous fins optimize the surface space used for heat exchange from the PV cells towards the PCM, resulting in quicker heating and greater thermal efficiency. During a period of time, efficiency maintains a steady level as the PCM captures heat, keeping the optimum PV temperature. Case D (PCM with porous fins) has a better potential for enhancing the thermal characteristics of PVT than a PCM system without porous fins. Due to enhanced heat transmission from the porous fins to the PCM, the effectiveness of the porous fin system stays steady even after full melting, offering superior thermal control. The mean improvement in thermal effectiveness for PVT with porous fins is approximately 16% when compared with the scenario without porous fins.

4.2 Influence of tilt angle on the efficacy of porous fins in the PVT-PCM system

This part analyses the impacts of changing tilt angles on the effectiveness of a PVT system. The system, which includes five porous fins, was tested under various circumstances at tilt angles of 0°, 30°, and 90°, with various melting periods. Visual representations of the liquid fracture profiles within the PVT system are supplied in Figure 10. A constant solar irradiance of 1000 W/m² on the upper surface of the PV module is assumed within the modelling setup. Therefore, gradual heating of the PCM placed under the PV cell occurs, with temperature elevation facilitated by conductive heat transfer from the PV cell. As time progresses, the porous fins serve a dual purpose: firstly, in enabling the extraction of entrapped thermal energy from the PV cell, and secondly, in inducing the onset of natural convection phenomena within the melted PCM domain. This augmentation in convective activity is particularly pronounced within the upper regions of the domain, owing to active buoyancy-driven dynamics in this region. The consequential outcome is the notable augmentation in liquid PCM content, visually identifiable as the "red zone." However, a noticeable departure in melting kinetics is discernible as the inclination angle is reduced below 90°, effectively transitioning towards the vertical orientation. This is due to a decrease in convective

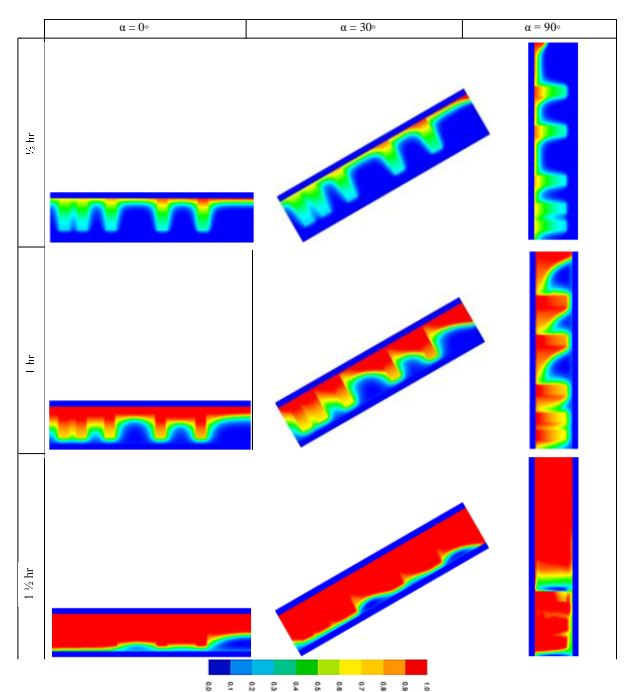


Fig 10. Contours for the liquid-fraction evolution over different periods of PCM melting with varying the inclination angle

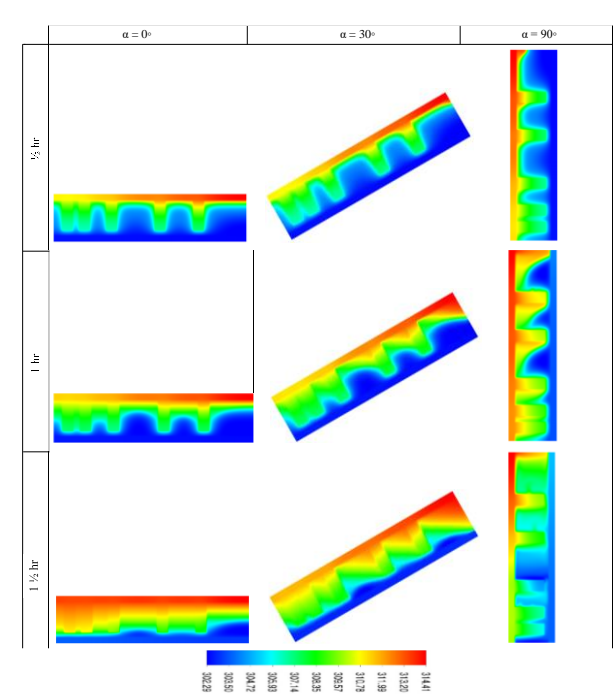


Fig 11. Contours for the temperature distribution over different periods of PCM melting with varying the inclination angle.

currents, resulting in a slower melting rate. This phenomenon is more noticeable after 1.5 hours of continuous melting. The extent of the molten layer is accentuated by the vertical orientation ($\alpha=90^{\circ}$), where an extensive melting domain is evident due to buoyancy-mediated fluid dynamics. Consequentially, a pivotal deduction is drawn, elucidating that inclination angles departing from 90° invariably indicate a diminishing trend in PCM melting rates across the entire system. This sensitivity to inclination angle is crucial in shaping PCM melting kinetics and dictating the potential for thermal management within the PVT system.

As for the temperature distribution, uniformity characterizes the isotherms in Figure 11 across different inclination cases during the initial half-hour period. This homogeneity arises from the considerable thermal output generated by the PV module during its operational phase, which is subsequently conveyed to the PCM through the presence of porous fins. This heat exchange mechanism fosters the establishment of marked temperature gradients proximate to both the PV panel and the porous fins. This phenomenon is visually evident in the discernible color field, encompassing shades of yellow to red, as depicted in Figure 11. These temperature gradients exhibit a progressive augmentation over time, particularly when the angle of inclination descends below 90°. Upon entering the subsequent hour, a noteworthy observation manifests—namely, the minimal gradient discerned within the red layer when the orientation stands at 90°. However, this specific condition stands in contrast to the pronounced thermal gradients observable across varying angular configurations. Notably, when the inclination angle of the PV panel dips beneath 90°, even with the integration of porous fins, a discernible temperature differential becomes conspicuous throughout the PCM domain. This variation adversely affects both the operational efficiency of the PCM and the heat dissipation performance facilitated by the porous fins within the PVT system.

The temporal evolution of the PCM liquid fraction within the PVT system, augmented with an arrangement of five porous fins, is graphically given in (Figure 12). Observably, alterations

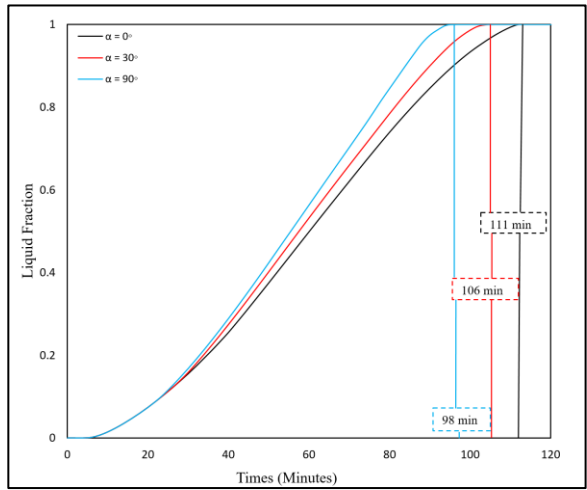


Fig 12. Liquid fraction variation over time for the PCM with porous fins

in the angle of PV tilt yield inconsequential differences during the initial phase ($t \le 30 \text{ min}$) of the melting process across all examined angles. However, as time progresses, discernible divergences manifest in the liquid fraction profiles, exhibiting augmented prominence as the inclination angles decrease. Quantitatively, the melting durations for the examined inclinations of 90°, 30°, and 0° amount to 98, 106 and 111 minutes, respectively. Evidently, transitioning the PV panel's inclination from 0° to 90° expeditiously accelerates the total melting duration by approximately 12%. This outcome underscores the pertinence of the inclination angle in accelerating the melting rate, thereby influencing the thermal management process. Consequently, the utilization of alternative angles within the PVT configuration can impede the PCM's melting progression, consequently prolonging the interval for which the cell temperature remains elevated and diminishing the effective PCM functionality. Notably, an inclination angle of about 90° emerges as a preferable configuration, correlating with the heightened melting efficiency of the PCM in charge.

4.3 Comparison with the reference case of solid fins

After analysing the results of the five porous fin in PVT-PCM system, the result proved that case D with a tilt angle of 90° was superior at lowering the cell temperature and accelerating the melting of PCM. This section compares the cell temperature control and PCM melting efficiency between Case D, which uses porous aluminium fins to another study Case uses the same dimensions but solid aluminium fins. The new case has a fin configuration similar to the one considered in previous literatures (Khanna, Reddy, & Mallick, 2018b; Zhang *et al.*, 2023)). The PCM melting and temperature variation fluctuations possibilities are demonstrated in Figure 13.

In the initial stage, at exactly 0.5 hour, the difference between melted PCM for porous fins and solid fins is the same with little difference in both scenarios. However, Figure 13 confirms that the time period of heat transfer from the PV cell to the PCM through the porous fins is more efficient than using solid fins due to the larger surface area of porous fins compared to solid fins. In addition, the interconnected pores promote heat transfer through convection, which improves heat dissipation and results in less liquid PCM during peak periods with a reduction in photocell temperature. When the PV system is not in use, the PCM can store additional thermal energy and provide more efficient thermal control by using latent heat. Therefore,

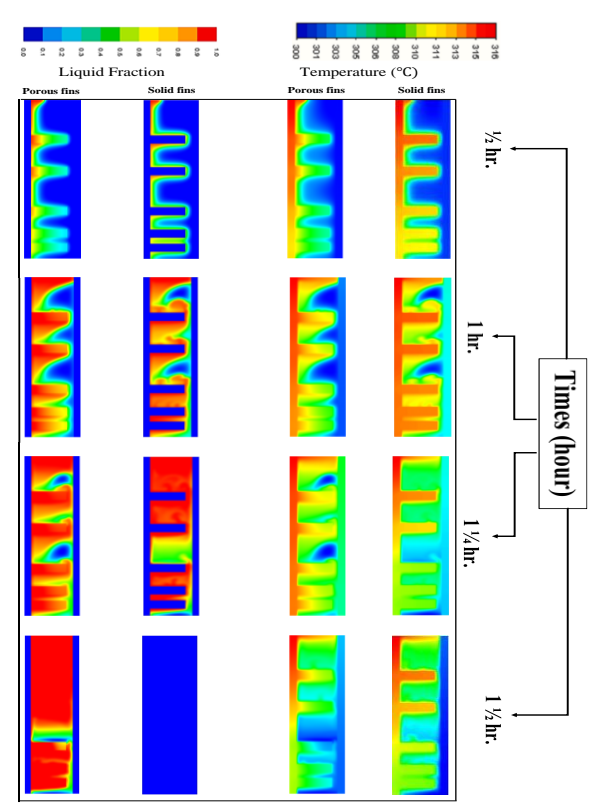


Fig 13. Liquid fraction (left), temperature (right) contours for porous and solid fins with PCM

after about 1.25 hours, the PCM in the solid fins dissolves more quickly than what is in the porous fins.

Figure 14 disclose key disparities between utilizing porous versus solid metallic fins for thermal regulation within the PVT system owing to considerable differences in heat transfer enhancement potential. The solid fins elicit appreciably faster bulk melting of the PCM, with total phase transition achieved in 86 minutes, a 12.2% reduction relative to the 98 minutes required with porous fins. This deviation stems from the solid fins' more limited surface area contact with the PCM medium which becomes less effective at extracting heat from the PV cell upon progression beyond the initial conductive regime. Consequently, with porous fins, the temperature undergoes more gradual modulation, prolonging the melting duration to provide longer thermal management duration on the PV side. Figure 15 conveys the temperature development over time for both systems. In the first period, both porous and solid fins facilitate efficient heat removal away from the PV cell, causing rapid early temperature rises until onset of PCM melting and subsequent heat absorption. This manifests in temperature stabilization with readings around 34°C for solid fins and 36°C for porous fins. Quantitatively, this reflects a 12.4% lower cell temperature for the solid fins at the 30-minute mark during the solid-liquid phase change progression. However, beyond this regime, the porous fins provide superior temperature regulation, keeping readings consistently around 36°C even after fully melting the PCM due to the good heat dissipation into the liquid phase PCM. In comparison, lacking such extensive heat transfer area, the solid fins elicit renewed temperature climbs potentially reaching 40°C upon PCM depletion, reducing PV electrical conversion efficiency. Thus, while enabling faster initial melting, solid fins provide inferior thermal regulation capabilities relative to porous fins on prolonged timescales requisite for long PVT operation.

In summary, the large surface area of the porous fins and the lightweight structure enabled better heat dissipation, lower

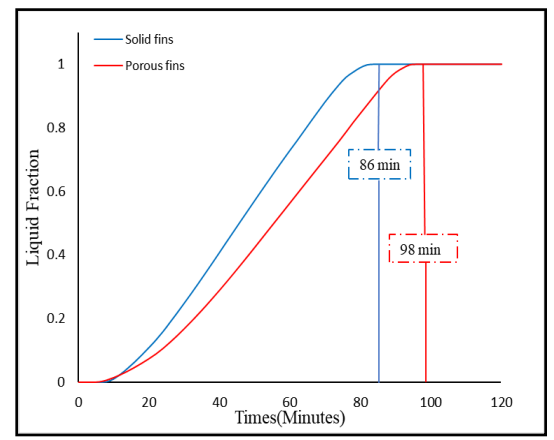


Fig 14. Liquid fraction of PCM with porous fins and solid fins over times

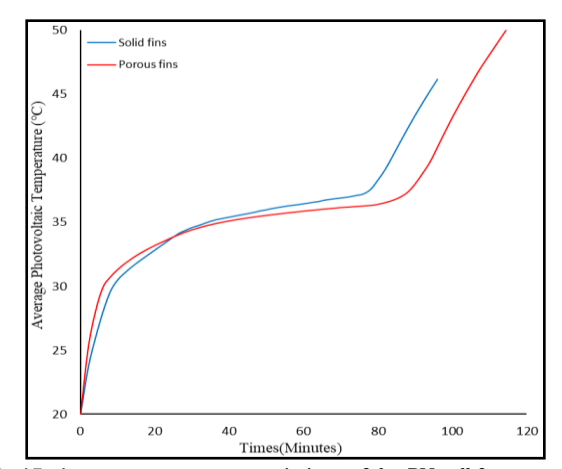


Fig 15. Average temperature variations of the PV cell for porous fin and solid fins

temperatures of the PV modules, and better temperature management of the PV cells. This combination can increase the efficiency and lifespan of the solar PV system.

5 Conclusion

This work explores a passive thermal regulation approach for PVT systems based on tailored porous fins embedded in PCM encapsulations. The results showed that the porous fin structures can provide efficient pathways to facilitate heat dissipation from the PV cells, enabling superior passive thermal regulation of the PVT system. An optimized staggered porous fin distribution (Case D) demonstrates the best thermal regulation performance in the PVT system, decreasing PV cell temperatures by 5°C and extending regulation time versus pure PCM. In addition, the porous fins boost PVT thermal efficiency by 16 % and electrical output by 2.98% over the non-finned baseline, show casing synergistic improvements. Further, tilting the finned PVT system from 0° to 90° curtails melting time by 13 minutes, elucidating angle sensitivity. Comparisons with solid fins indicate a 12.24% reduction in melting duration but compromised thermal management capabilities. In closure, the porous fin structures develop conductive pathways to facilitate heat dissipation from the PV cells and enable better passive thermal regulation of the PVT system. The design delivers simultaneous advancements in thermal management and electrical performance compared to traditional PVT collectors, achieved through the strategic incorporation of porous media.

The findings would guide system optimization and upscaling to satisfy more efficient sustainable energy solutions.

Nomenclature

A_{mushy}	Mushy	area	factor	(10^5)	

- A_{sf} The surface area for porous cells with length. (m-1)
- C_f C_p Inertial factor of porous cells (m-1)
- Specific heat amplitude (J/kg K)
- d_l Ligament diameter for porous cells (m)
- Pore the diameter for porous cells (m) d_p
- Acceleration (m/s2)
- g h Heat transfer parameter(W/m² K)
- Н Enthalpy parameter (J/kg)
- Ι Solar radiation level (W/m²)
- k Thermal Conductivity parameter (W/m K)
- K Permeability for porous cells (m-2)
- L Latent heat parameter (J/kg)
- Pressure (Pa)
- PrPrandtl number factor
- Ra Rayleigh number factor
- TTemperature (K)
- T_{glass} Glass Temperature (K)
- T_{sky} Sky Temperature (K)

Greek Symbols

- Liquid Fraction λ
- Density(kg/m³) ρ
- Dynamic viscosity parameter (kg/m s) μ
- β Thermal expansion parameter
- ε Porosity (non-dimensional)
- Pore density (PPI) ω
- α tilt angle (dimensionless)

Subscripts

Aluminium Ambient amb Inlet

init Initial

Liquid, solid phase l, s forced Forced convection free Free convection рст Phase change material

Abbreviations

Photovoltaic thermal CPVConcentrator photovoltaic PVPhotovoltaic panel PCMPhase change material PPIPore number per inch

References

- Al-Aasama, A. B., Ibrahim, A., Syafiq, U., Sopian, K., Abdulsahib, B. M., & Dayer, M. (2023). Enhancing the performance of water-based PVT collectors with nano-PCM and twisted absorber tubes [PVT-PCM; Twisted absorber tube; Nano-PCM; Photovoltaic thermal efficiency; Primary Energy Saving efficiency]. International Journal of Renewable Energy Development, 12(5), https://doi.org/https://doi.org/10.14710/ijred.2023.54345
- Al-Waeli, A. H., Kazem, H. A., Chaichan, M. T., & Sopian, K. (2019). Photovoltaic/thermal (PV/T) systems: principles, design, and applications. Springer Nature.
- Al-Waeli, A. H., Sopian, K., Chaichan, M. T., Kazem, H. A., Ibrahim, A., Mat, S., & Ruslan, M. H. (2017). Evaluation of the nanofluid and nano-PCM based photovoltaic thermal (PVT) system: An experimental study. Energy conversion and management, 151, 693
 - https://doi.org/https://doi.org/10.1016/j.enconman.2017.09.0
- Al-Waeli, A. H., Sopian, K., Kazem, H. A., Yousif, J. H., Chaichan, M. T., Ibrahim, A., Mat, S., & Ruslan, M. H. (2018). Comparison of prediction methods of PV/T nanofluid and nano-PCM system using a measured dataset and artificial neural network. Solar 162, 378-396. Energy, https://doi.org/https://doi.org/10.1016/j.solener.2018.01.026

- Bergman, T. L., Bergman, T. L., Incropera, F. P., Dewitt, D. P., & Lavine, A. S. (2011). Fundamentals of heat and mass transfer. John Wiley &
- Biwole, P. H., Eclache, P., & Kuznik, F. (2013). Phase-change materials to improve solar panel's performance. Energy and Buildings, 62, 59-

https://doi.org/https://doi.org/10.1016/j.enbuild.2013.02.059

- Calmidi, V. V., & Mahajan, R. L. (2000). Forced convection in high porosity metal foams. J. Heat Transfer, 122(3), 557-565. https://doi.org/https://doi.org/10.1115/1.1287793
- Cheong Tan, W., Huat Saw, L., San Thiam, H., Yusof, F., Wang, C.-T., Chian Yew, M., & Kun Yew, M. (2019). Investigation of water cooled aluminium foam heat sink for concentrated photovoltaic solar cell. IOP Conference Series: Earth and Environmental Science,
- Duan, J. (2021). A novel heat sink for cooling concentrator photovoltaic system using PCM-porous system. Applied Thermal Engineering, 116522. https://doi.org/https://doi.org/10.1016/j.applthermaleng.2020 .116522
- GmbH., R. https://www.rubitherm.eu. https://www.rubitherm.eu.
- Indartono, Y., Prakoso, S., Suwono, A., Zaini, I., & Fernaldi, B. (2015). Simulation and experimental study on effect of phase change material thickness to reduce temperature of photovoltaic panel. IOP Conference Series: Materials Science and Engineering, 88(1), 012049. https://doi.org/10.1088/1757-899X/88/1/012049
- Jamil, F., Ali, H. M., Nasir, M. A., Karahan, M., Janjua, M., Naseer, A., Ejaz, A., & Pasha, R. A. (2021). Evaluation of photovoltaic panels using different nano phase change material and a concise comparison: An experimental study. Renewable Energy, 169, 1265-1279. https://doi.org/10.1016/j.renene.2021.01.089
- Kant, K., Shukla, A., Sharma, A., & Biwole, P. H. (2016). Thermal response of poly-crystalline silicon photovoltaic panels: Numerical simulation and experimental study. Solar Energy, 134,

https://doi.org/https://doi.org/10.1016/j.solener.2016.05.002

- Kaplani, E., & Kaplanis, S. (2014). Thermal modelling and experimental assessment of the dependence of PV module temperature on wind velocity and direction, module orientation and inclination. Energy, https://doi.org/https://doi.org/10.1016/j.solener.2014.05.037
- Khanna, S., Reddy, K., & Mallick, T. K. (2018a). Effect of climate on electrical performance of finned phase change material integrated photovoltaic. Solar Energy, 174, https://doi.org/https://doi.org/10.1016/j.solener.2018.09.023
- Khanna, S., Reddy, K., & Mallick, T. K. (2018b). Optimization of finned solar photovoltaic phase change material (finned pv pcm) system. International Journal of Thermal Sciences, 130, 313-322. https://doi.org/https://doi.org/10.1016/j.ijthermalsci.2018.04. 033
- Kılkış, B. (2020). Development of a composite PVT panel with PCM embodiment, TEG modules, flat-plate solar collector, and thermally pulsing heat pipes. Solar Energy, 200, 89-107. https://doi.org/https://doi.org/10.1016/j.solener.2019.10.075
- Li, J., Zhang, W., Xie, L., Li, Z., Wu, X., Zhao, O., Zhong, J., & Zeng, X. (2022). A hybrid photovoltaic and water/air based thermal (PVT) solar energy collector with integrated PCM for building application. Renewable Energy, 199. 662-671. https://doi.org/https://doi.org/10.1016/j.renene.2022.09.015
- Ma, T., Yang, H., Zhang, Y., Lu, L., & Wang, X. (2015). Using phase change materials in photovoltaic systems for thermal regulation and electrical efficiency improvement: A review and outlook. Renewable and Sustainable Energy Reviews, 43, 1273-1284. https://doi.org/https://doi.org/10.1016/j.rser.2014.12.003
- Ma, Z., Lin, W., & Sohel, M. I. (2016). Nano-enhanced phase change materials for improved building performance. Renewable and Sustainable Energy Reviews, 58, 1256-1268.
- Maatallah, T., Zachariah, R., & Al-Amri, F. G. (2019). Exergo-economic analysis of a serpentine flow type water based photovoltaic thermal system with phase change material (PVT-PCM/water). Solar Energy, 193, 195-204. https://doi.org/https://doi.org/10.1016/j.solener.2019.09.063
- Mahdi, J. M., Lohrasbi, S., Ganji, D. D., & Nsofor, E. C. (2018). Accelerated melting of PCM in energy storage systems via novel configuration of fins in the triplex-tube heat exchanger.

- International Journal of Heat and Mass Transfer, 124, 663-676. https://doi.org/https://doi.org/10.1016/j.ijheatmasstransfer.20 18 03 095
- Mahdi, J. M., Mohammed, H. I., & Talebizadehsardari, P. (2021). A new approach for employing multiple PCMs in the passive thermal management of photovoltaic modules. *Solar Energy*, 222, 160-174. https://doi.org/https://doi.org/10.1016/j.solener.2021.04.044
- Mahdi, J. M., & Nsofor, E. C. (2018). Multiple-segment metal foam application in the shell-and-tube PCM thermal energy storage system. *Journal of Energy Storage*, 20, 529-541. https://doi.org/https://doi.org/10.1016/j.est.2018.09.021
- Mahdi, J. M., Singh, R. P., Al-Najjar, H. M. T., Singh, S., & Nsofor, E. C. (2021). Efficient thermal management of the photovoltaic/phase change material system with innovative exterior metal-foam layer. Solar Energy, 216, 411-427. https://doi.org/https://doi.org/10.1016/j.solener.2021.01.008
- Nada, S., El-Nagar, D., & Hussein, H. (2018). Improving the thermal regulation and efficiency enhancement of PCM-Integrated PV modules using nano particles. *Energy conversion and management*, 166, 735-743. https://doi.org/https://doi.org/10.1016/j.enconman.2018.04.0 35
- Nižetić, S., Jurčević, M., Arıcı, M., Arasu, A. V., & Xie, G. (2020). Nanoenhanced phase change materials and fluids in energy applications: A review. Renewable and Sustainable Energy Reviews, 129, 109931.
- Ren, Q., Xu, H., & Luo, Z. (2019). PCM charging process accelerated with combination of optimized triangle fins and nanoparticles. *International Journal of Thermal Sciences*, 140, 466-479. https://doi.org/https://doi.org/10.1016/j.enconman.2018.04.0 35
- Shakibi, H., Afzal, S., Shokri, A., & Sobhani, B. (2022). Utilization of a phase change material with metal foam for the performance improvement of the photovoltaic cells. *Journal of Energy Storage*, 51, 104466. https://doi.org/https://doi.org/10.1016/j.est.2022.104466
- Sharaf, M., Huzayyin, A., & Yousef, M. S. (2022). Performance enhancement of photovoltaic cells using phase change material (PCM) in winter. *Alexandria Engineering Journal*, *61*(6), 4229-4239. https://doi.org/https://doi.org/10.1016/j.aej.2021.09.044
- Sharma, S., Micheli, L., Chang, W., Tahir, A., Reddy, K., & Mallick, T. (2017). Nano-enhanced Phase Change Material for thermal

- management of BICPV. Applied Energy, 208, 719-733. https://doi.org/10.1016/j.apenergy.2017.09.076
- Skoplaki, E., & Palyvos, J. A. (2009). Operating temperature of photovoltaic modules: A survey of pertinent correlations. *Renewable Energy*, 34(1), 23-29. https://doi.org/https://doi.org/10.1016/j.renene.2008.04.009
- Tan, L., Date, A., Fernandes, G., Singh, B., & Ganguly, S. (2017). Efficiency gains of photovoltaic system using latent heat thermal energy storage. *Energy Procedia*, 110, 83-88.
- Thaib, R., Rizal, S., Mahlia, T., & Pambudi, N. A. (2018). Experimental analysis of using beeswax as phase change materials for limiting temperature rise in building integrated photovoltaics. *Case Studies in Thermal Engineering*, 12, 223-227. https://doi.org/https://doi.org/10.1016/j.csite.2017.12.005
- Tian, Y., & Zhao, C.-Y. (2011). A numerical investigation of heat transfer in phase change materials (PCMs) embedded in porous metals. *Energy*, 36(9), 5539-5546. https://doi.org/https://doi.org/10.1016/j.csite.2023.103825
- Waqas, A., & Ji, J. (2017). Thermal management of conventional PV panel using PCM with movable shutters—A numerical study. *Solar Energy*, 158, 797-807. https://doi.org/https://doi.org/10.1016/j.solener.2017.10.050
- Waqas, A., Ji, J., Xu, L., Ali, M., & Alvi, J. (2018). Thermal and electrical management of photovoltaic panels using phase change materials—A review. Renewable and Sustainable Energy Reviews, 92, 254-271.
 - https://doi.org/https://doi.org/10.1016/j.rser.2018.04.091
- Waqas, A., Jie, J., & Xu, L. (2017). Thermal behavior of a PV panel integrated with PCM-filled metallic tubes: An experimental study. *Journal of Renewable and Sustainable Energy*, 9(5), 053504. https://doi.org/10.1016/j.solener.2017.10.050
- Xu, Y., Ren, Q., Zheng, Z.-J., & He, Y.-L. (2017). Evaluation and optimization of melting performance for a latent heat thermal energy storage unit partially filled with porous media. applied energy, 193, 84-95. https://doi.org/https://doi.org/10.1016/j.apenergy.2017.02.01
- Zhang, C., Wang, N., Xu, H., Fang, Y., Yang, Q., & Talkhoncheh, F. K. (2023). Thermal management optimization of the photovoltaic cell by the phase change material combined with metal fins. *Energy*, 263, 125669. https://doi.org/https://doi.org/10.1016/j.energy.2022.125669



© 2024. The Author(s). This article is an open access article distributed under the terms and conditions of the Creative Commons Attribution-ShareAlike 4.0 (CC BY-SA) International License (http://creativecommons.org/licenses/by-sa/4.0/)